Experimental identification of effective mass transport models in falling film flows

P. Bandi[†], S. Groß[‡], M. Karalashvili[*], A. Mhamdi[*], H. Pirnay[*], L. Zhang[‡], W. Marquardt[*], M. Modigell[†], A. Reusken[‡]

In many industrial units (e.g. packing columns, falling film reactors), the liquid phase is designed as a falling film, since it is well known that the mass and heat transfer in laminar-wavy film flows is significantly enhanced. Computational design models which account for these enhanced transport mechanisms are necessary. The numerical simulation of the coupled momentum and mass transport equations is computationally infeasible due to its multiphase nature and the dynamic, unstable interface. To overcome this problem, we propose a transport model based on effective diffusion coefficients and suggest an incremental approach for its identification. This incremental approach is computationally feasible while still accounting for the wave-induced transport intensification. The model identification is based on high-resolution concentration measurements of oxygen being physically absorbed into an aqueous film applying a planar laser-induced luminescence (pLIL) measurement technique. Preliminary measurement and estimation results are presented.

Keywords. Falling film, mass transport, effective diffusion coefficient, incremental identification, concentration measurements, numerical simulation.

1 Introduction

In industrial applications such as CO_2 scrubbers, falling film evaporators, absorption heat pumps as well as many others, falling films are widely used. In these devices the liquid phase occurs as a gravity driven thin film. The heat and mass transport properties in these films are significantly intensified by their waviness [4]. The dynamic and complex structure of the film complicate its detailed experimental and numerical analysis. Therefore, falling films are subject to ongoing research efforts (see [9, 17, 22, 23, 27] and the references therein). Despite these efforts, the understanding of the transport phenomena is still limited and comprehensive transport models are not available.

The direct numerical treatment of first principle models for mass transport inside the film require the simultaneous solution of the two-phase Navier-Stokes equations of the gas and liquid phase. In available simulations, unphysical effects are often observed, leading to the conclusion that today's numerical tools are not mature enough to be relied upon.

[*]Process Systems Engineering, RWTH Aachen, Germany
[†]Mechanical Process Engineering, RWTH Aachen, Germany
[‡]Chair for Numerical Mathematics, RWTH Aachen, Germany

These observations show that there is a need for *reduced design models*, which are capable of modeling the defining properties of the transport phenomena in falling films while keeping the computational demand down to a minimum.

In this work, a transport model for liquid falling films based on effective diffusion coefficients is proposed. The model will be identified using incremental model-based identification. This approach calls for a close collaboration between experiments, numerics and modeling. Examples for this collaboration are the development of stabilization methods in the inverse problems of the identification and the application of model-based image processing to the experimental data.

By combining these complementary expertises, a versatile systematic toolbox is created. In this paper we describe the main ideas underlying our interdisciplinary approach fo deriving an effective mass transport model in falling film flows.

The paper is organized as follows. First, the modeling approach is described in detail, focusing on the derivation of the reduced model. This is followed by an explanation of the numerical methods employed, focusing on stabilization for convection-dominated problems, as well as the solution of PDEs on wavy computational domains. The pLIL measurement technique, as well as the experimental setup is introduced in the third part. First results of the joint work are presented.

2 Incremental Modeling and Identification

In this section, a transport model for liquid falling films based on effective diffusion coefficients is proposed. First, the reduced flow model used for the convection-diffusion equations emerging in these problems is described. Then, the model structure is derived using the incremental method. For the subsequent model identification, the incremental method is employed. Finally, the solution of the inverse problems appearing in the model identification is outlined.

2.1 One-phase wavy film model

As described above, the direct numerical simulation of the Navier-Stokes equations for the two-phase flow model of the liquid and gas phase is currently infeasible and even in the longer run impractical in an industrial environment. Therefore, the detailed two-phase flow model is replaced by a reduced one-phase flow model of the liquid phase. The film height $\delta(x, z, t)$ of the wavy film is computed from an evolution equation based on the Long-Wave theory. We employ a two-equation expansion of the film thickness δ and the volume flow rate $\dot{V}$ in the film. These expansions have been shown to accurately describe the film for a wide range of flow regimes [21].

The velocity profile $\mathbf{u}$ inside the film is computed from $\dot{V}$, by assuming a parabolic velocity profile. The three parameters of this parabolic profile are determined by the mass balance, no-slip condition at the wall, and vanishing shear-stress at the free boundary. Note that as opposed to the flat-film solution (Nusselt solution) of the film profile used in previous studies [14], the flow conditions defined by δ and $\mathbf{u}$ do not necessarily satisfy the Navier-Stokes equations. However, they are an easily obtainable, reasonable approximation and yield a more accurate description of the state of the film.

Using the film height δ, the time-dependent computational domain $\Omega_f(t)$ is defined as

$$\Omega_f(t) = \{\ (x, y, z) \in \mathbb{R}^3 \mid 0 < y < \delta(x, z, t), x \in (0, L_x), z \in (0, L_z)\ \}. \tag{1}$$

All PDEs introduced in the following sections will be defined on the set $\Omega_f(t)$.

2.2 Incremental Modeling

In order to achieve transparency in the modeling procedure, the incremental method as described by [19, 20] is applied. Starting point for the incremental procedure is the generic transient balance equation

$$c_t + \nabla \cdot \mathbf{J} = 0, \tag{2}$$

where $\mathbf{J}$ is the overall molecular flux and c_t is the derivative of the concentration w.r.t. time. $\mathbf{J}$ can be separated into a convective term induced by the velocity field $\mathbf{u}$ and a diffusive term $\mathbf{J}_D$,

$$\mathbf{J} = c\mathbf{u} + \mathbf{J}_D. \tag{3}$$

Using (2) and the fact that $\nabla \cdot \mathbf{u} = 0$ for incompressible fluids, this leads to

$$c_t + \mathbf{u} \cdot \nabla c + \nabla \cdot \mathbf{J}_D = 0. \tag{4}$$

Note that in this modeling step the diffusion term $\mathbf{J}_D$ is not yet specified. The decision on a model for $\mathbf{J}_D$ follows in the next step. We assume a flux according to Fick's law

$$\mathbf{J}_D = -D_{\text{eff}} \nabla c, \tag{5}$$

where D_{eff} is the unknown, state dependent diffusion coefficient. This diffusion coefficient is further divided into the contribution of the molecular diffusion D_{mol} and effects due to the waviness of the film D_{w},

$$D_{\text{eff}} = D_{\text{mol}} + D_{\text{w}}. \tag{6}$$

The molecular diffusion D_{mol} is constant and known from the literature. The wavy diffusion coefficient D_{w} is unknown, and is introduced to describe the enhancement of mass transport due to the waviness in the film. On the final level of detail in the modeling process, a model for D_{w} is specified. As nothing is known a priori of the wavy diffusion coefficient, we postulate a general model

$$D_{\text{w}}(x, y) = f_{\text{w}}\left(c, x, t, \theta\right) \tag{7}$$

with model parameters $\theta \in \mathbb{R}^n$.

The procedure outlined above for the incremental modeling of mass transfer can be applied in the same way to the problem of heat transfer in the falling film [14]. The boundary conditions, however, are different for every experimental setup. The conditions used in our study of transport of oxygen from the gas into the liquid phase are as follows. In our setup (cf. Figure 3), we set a Dirichlet condition for the concentration at the inlet boundary Γ_{in}. The value of this concentration is taken from measurements of the inlet chamber. The surface boundary Γ_{surf} is modeled as a Dirichlet boundary, as well. We assume that the limiting process is the transport within the liquid phase. Therefore, the concentration at the boundary is set to the equilibrium concentration corresponding to the concentration in the gas phase. The remaining boundaries are modeled using zero-flux Neumann conditions. The location of the boundaries is illustrated in Figure 3.

2.3 Incremental Identification

The structure and parameters of the function f_{w} introduced in (7) are identified using the method of incremental identification. The identification closely follows the steps of the incremental modeling procedure. In a first step, the generic diffusive flux $\mathbf{J}_D$ is identified. To make this problem numerically more tractable, we introduce a source term $F_{\mathrm{eff}} = -\nabla \cdot \mathbf{J}_D = \nabla \cdot (D_{\mathrm{mol}} \nabla c) + F_{\mathrm{w}}$, yielding

$$c_t + \mathbf{u} \cdot \nabla c = F_{\mathrm{eff}}. \tag{8}$$

For reasons of numerical stability, the molecular diffusion is included into the left-hand side of the equation,

$$c_t + \mathbf{u} \cdot \nabla c - \nabla \cdot (D_{\mathrm{mol}} \nabla c) = F_{\mathrm{w}}, \tag{9}$$

with F_{w} representing the divergence of the wavy part of $\mathbf{J}_D$. Given the high resolution distributed concentration measurements c_m obtained in the experiments, the source term F_{w} is identified. In a second step, the wavy diffusion coefficient is inferred from the definition of the source term

$$-\nabla \cdot (D_{\mathrm{w}} \nabla c) = -F_{\mathrm{w}}. \tag{10}$$

Note that the source term only accounts for the enhanced diffusion induced by D_{w}, as the molecular diffusion was included to convert (8) into a parabolic PDE. An important feature of this equation is the fact that the time does not appear explicitly. After D_{w} and thus D_{eff} has been identified from (10), the model structure f_{w} can be identified using finite-dimensional nonlinear optimization methods.

The full modeling and identification procedure is illustrated in Figure 1. The model identification approach described here has several advantages over the method of direct identification of the parameters θ from the full model

$$c_t + \mathbf{u} \cdot \nabla c - \nabla \cdot ((D_{\mathrm{mol}} + f_{\mathrm{w}}(\theta)) \nabla c) = 0. \tag{11}$$

One of the main challenges of this full model identification problem is that the structure of the model f_{w} is completely unknown. To identify the correct structure, the full-scale nonlinear instationary problem (11) would have to be solved for each model candidate. In the incremental approach presented above, the parameters of the model are only identified in the final step. This means that the time consuming step of discriminating among a large set of candidate models does not have to be done in the context of an inverse PDE problem, but instead in the much simpler framework of function approximation.

2.4 Solution of the inverse problems

In the incremental method described above, a series of consecutive inverse problems has to be solved. As the balance equations for heat and mass transfer are very similar, we use the same methods here as in previous studies on the identification of heat transfer in wavy films [15, 16].

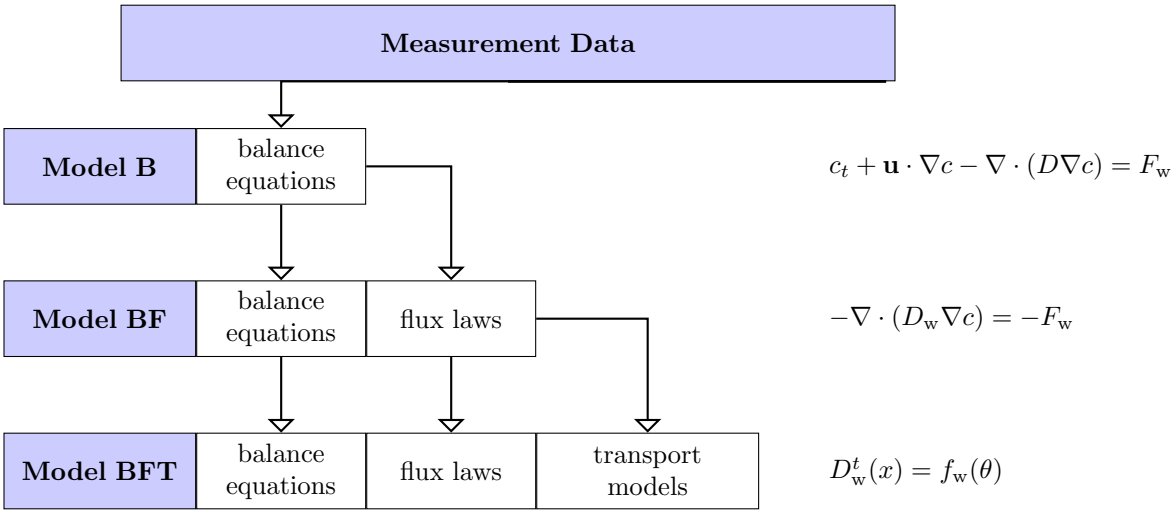

Figure 1: Incremental modeling and identification of mass transport

2.4.1 The source inverse problem

The first inverse problem in this sequence is the estimation of the source term F_w from measurements c_m. This problem is framed as an optimization problem. Let

$$K_1 : \mathcal{L}^2 \to \mathcal{L}^2,\ F_\mathrm{w} \mapsto c(F_\mathrm{w})$$

denote the operator that maps a source term F_w to the corresponding concentration profile c. In this case, K_1 is implicitly defined by (9). The inverse problem can be written as the optimization problem

$$\text{(IA1)} \quad \min_{F_\mathrm{w}} \|K_1(F_\mathrm{w}) - c_m\|_{\mathcal{L}^2}^2, \tag{12}$$

where c_m is a set of measurement data for the concentration c. Since K_1 is linear, this problem can be solved reliably using the CGNE algorithm. The regularization in this context is achieved by a suitable choice of the number of iterations of the CGNE algorithm [8, 11].

In the spirit of the theory of inverse problems, we call the application of K_1 to an element F_w - in other words the solution of the PDE (9) - the direct problem. The CGNE algorithm needs the evaluation of the sensitivity and adjoint operators corresponding to K_1 in every iteration. These operators are given by PDEs of the form (9) only with different coefficient functions and boundary conditions [13].

2.4.2 The coefficient inverse problem

The second inverse problem of the identification procedure is the estimation of the wavy diffusion coefficient D_w given the source term F_w. Let

$$K_2 : \mathcal{L}^2 \to \mathcal{L}^2,\ D_\mathrm{w} \mapsto c(D_\mathrm{w})$$

denote the operator implicitly defined by (10), where the solution F_w^* of (12) is used as the right-hand side. Note that the corresponding PDE is time-independent. Therefore, the

solutions to different time steps can be decoupled and the problem is solved for each time step independently.

After the decoupling of the time steps, n_t problems of the type

$$\text{(IA2)} \quad \min_{D_{\mathrm{w}}^t} \|K_2(D_{\mathrm{w}}^t) - c_m^t\|_{\mathcal{L}^2}^2 \tag{13}$$

need to be solved, where n_t is the number of time steps, c_m^t denotes the concentration measurement data at time t and the superscript t indicates the value of a function at time t. For these nonlinear inverse problems, we use the truncated Newton CG algorithm described in [11].

2.4.3 Correction step and parametric model identification

One drawback of the incremental method is that errors introduced in one identification step propagate directly into all following steps. In (IA2), D_{w} is estimated using the solution F_{w}^* of the previous source-inverse problem. Any error introduced in F_{w}^* will therefore influence the solution D_{w}^* as well. To damp this propagation of error, a so-called correction step is performed to reconcile the solution with the measurements. The correction step is the solution of the inverse problem

$$\text{(IA12)} \quad \min_{D_{\mathrm{w}}} \|K_{12}(D_{\mathrm{w}}) - c_m\|_{\mathcal{L}^2}^2 \tag{14}$$

where K_{12} is implicitly defined by the PDE

$$c_t + \mathbf{u} \cdot \nabla c - \nabla \cdot ((D_{\mathrm{mol}} + D_{\mathrm{w}}) \nabla c) = 0 \tag{15}$$

with the usual boundary conditions. It is important to note that this is much easier after having solved (IA2), since the uncorrected solutions D_{w} of (IA2) serve as good initial values for the Newton-CG algorithm.

After the wavy coefficient has been found, a parametric model $D_{\mathrm{w}} = f_{\mathrm{w}}(\theta)$ is identified. This is again done through an optimization problem minimizing the mismatch between the model f_{w} and data D_{w}. This problem can be framed in the form of a nonlinear optimization problem

$$\min_{\theta} \|D_{\mathrm{w}}^i - f(c^i, x^i, t^i, \theta)\|_2. \tag{16}$$

by regarding the value D_{w}^i each grid point i at which D_{w} is available as a data point.

3 Numerical Simulation

Concerning the numerical simulation tool used in this project we distinguish two classes of methods. Firstly, for the identification steps described in Section 2, sufficiently accurate solutions to the PDEs representing the direct, sensitivity, and adjoint sensitivity operators are needed. Secondly, as a long-term goal the simulation of the fully three-dimensional two-phase flow model can be used as input (simulated, artificial data) for the identification procedure. If the full-scale simulation can achieve a good agreement with the experimental data, these simulations could serve as an valuable source of high resolution measurements. This second goal, however, is beyond the scope of this paper and will not be further addressed here.

All direct, sensitivity, and adjoint problems are of either elliptic or parabolic (convection-diffusion) type. Hence, similar numerical techniques can be employed for their solution. To this end, we employed the FEM code DROPS [7, 10]. DROPS is based on multilevel nested grids and conforming finite element discretization methods (FEM). For time discretization, a standard one-step θ-method is used. For the space discretization, piecewise linear finite elements on a tetrahedral grid are employed. The resulting discrete systems of linear equations are solved by suitable Krylov subspace methods. In case of the convection-diffusion equations, we use a preconditioned generalized minimal residuals (GMRES) method [24]. For the diffusion problems, a preconditioned CG method is applied.

In the following, we will address two specific issues that are important for an efficient incremental identification algorithm.

3.1 Stabilization of convection-dominated problems

Consider the convection-diffusion equation (9) with the source term $F_{\mathrm{w}}(\mathbf{x}, t)$ which is the direct problem in (IA1) above. The molecular diffusion parameter $D_{\mathrm{mol}} = \mathcal{O}(10^{-9})m^2/s$ is relatively small in our applications. For falling film problems, the ratio $\frac{\|\mathbf{u}\|_2}{D_{\mathrm{mol}}}$ is of the order $\mathcal{O}(10^7 \backsim 10^8)$. Even if we use very fine grids, with mesh size denoted by h, the Péclet number $Pe = \frac{h\|\mathbf{u}\|_2}{2D_{\mathrm{mol}}}$ is still much larger than 1. It is well-known that for standard FEM in convection-dominated problems oscillations may appear at boundary layers due to the lack of upwinding in standard FEM. The outflow boundary condition at Γ_{out} does not cause a boundary layer in the solution, but a boundary layer may appear at the wavy free surface. Besides that, in the adjoint problem for (IA1) the flow direction is reversed which means that we have Dirichlet boundary conditions at the outflow Γ_{in}. In this case numerical oscillations are observed if suitable stabilization techniques are not employed.

Furthermore, in a strongly convection-dominated problem iterative solvers are often slow, because the resulting linear systems have matrices with large condition numbers and eigenvalues with large imaginary parts. Introducing a stabilization in the discretization helps to reduce numerical oscillations and to improve relevant matrix properties.

Among the various stabilization techniques for FEM, we choose the streamline upwind Petrov-Galerkin (SUPG) method [5], which has been implemented in DROPS. This led to a significant decrease in computation times for convection dominated problems. In addition, a reduction of oscillations for the adjoint problem was observed.

3.2 Arbitrary Lagrangian-Eulerian techniques for free surface

To handle the time-dependent domain $\Omega_f(t)$ defined in (1) we use an Arbitrary Lagrangian-Eulerian approach (ALE) [3, 6, 18]. We assume that the local time-dependent film thickness $\delta(x, z, t)$ is a known quantity which has been calculated based on the Long-Wave Theory, cf. Section 2.1. Let $\hat{\Omega}$ be a fixed reference domain and $\Phi : \hat{\Omega} \times (0, T) \to \mathbb{R}^d$ a deformation function such that (cf. Fig. 2)

$$\Omega_f(t) = \{\mathbf{x} = \Phi^t(\hat{\mathbf{x}}) := \Phi(\hat{\mathbf{x}}, t) : \hat{\mathbf{x}} \in \hat{\Omega}\} \qquad \text{for all } t \in (0, T). \tag{17}$$

Due to the fact that the height of the free surface is an a-priori known function $\delta(x, z, t)$, the deformation of grids can therefore be achieved by a simple transformation of the y-coordinate.

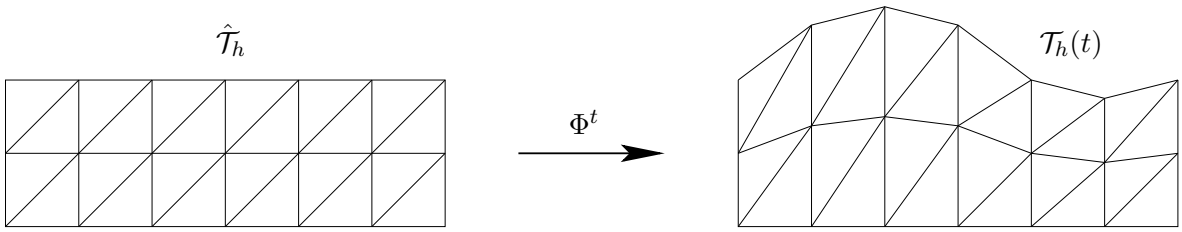

Figure 2: Transformation from the triangulation $\hat{\mathcal{T}}_h(t)$ on the reference domain $\hat{\Omega}$ to the triangulation $\mathcal{T}_h(t)$ on the moving domian $\Omega_f(t)$ through the transformation Φ^t

The partial differential equation to be solved is given by

$$c_{t,\hat{\Omega}} + (\mathbf{u} - \mathbf{u}_\Omega) \cdot \nabla c - \nabla \cdot (D_{\text{mol}} \nabla c) = F_{\text{w}} \qquad \text{in } \Omega_f(t), t \in [t_0, t_f], \tag{18}$$

where $c_{t,\hat{\Omega}}(\mathbf{x}, t) := \lim_{\Delta t \to 0} \frac{\hat{c}(\hat{\mathbf{x}}, t+\Delta t) - \hat{c}(\hat{\mathbf{x}}, t)}{\Delta t}$ with $\mathbf{x} = \Phi^t(\hat{\mathbf{x}})$ means the time derivative w.r.t. the fixed reference domain $\hat{\Omega}$ and

$$\mathbf{u}_\Omega(\mathbf{x}, t) = \dot{\mathbf{x}}(t) = (0, \frac{y}{\delta} \frac{\partial \delta(x, z, t)}{\partial t}, 0) \tag{19}$$

is the grid velocity of the moving grid $\mathcal{T}_h(t)$. Note that (18) is of the same structure as (9), and can therefore be treated with the same numerical methods.

4 Experimental Investigation

The highly resolved experimental data are obtained using the planar laser induced luminescence measuring technique (pLIL), which is a further development of the laser induced luminescence technique (LIL) introduced in [25], and enables simultaneous 2D concentration or temperature and film thickness measurements.

4.1 Measuring Method

The pLIL measuring method uses diacetyl (2,3-butanedione) as an optical indicator. In aqueous solutions diacetyl emits fluorescence and phosphorescence upon excitation with UV-light. The intensities of these emissions depend on incident laser energy, temperature and indicator concentration. In addition to that, the phosphorescence is quenched by dissolved oxygen, while the fluorescence emission is not affected by it. Based on these interrelations, it is possible to either determine the concentration distribution of absorbed oxygen in isothermal, laminar wavy films [25], or a temperature distribution within oxygen free films [26]. After a pulsed excitation with UV-light, the phosphorescence emission I decays according to

$$I(c, \vartheta, t) = I_0(c, \vartheta) e^{-t/\tau(c,\vartheta)}, \tag{20}$$

where I_0 denotes the initial phosphorescence intensity after turning off the laser and τ is the mean lifetime of the phosphorescence. In this work only isothermal films ($\vartheta = \text{const}$) are considered. Therefore, the phosphorescence emission is a function of only the oxygen concentration c.

The dissolved oxygen acts as a physical quencher and reduces not only the lifetime, but also the initial intensity of the phosphoresence. This correlation is given by the Stern-Volmer equation

$$\frac{\tau}{\tau_0} = \frac{I_0}{I_0^*} = \frac{1}{1 + c/c_h}. \tag{21}$$

In this equation I_0^* and τ_0 are the initial intensity and the mean lifetime of the phosphorescence in an oxygen-free solution. I_0 and τ relate to the same quantities according to the oxygen concentration in the system. The parameter c_h is the half-value concentration.

Combination of (20) and (21) yields a formulation of the phosphorescence decay as a function of the local oxygen concentration,

$$\frac{I}{I_0^*} = \frac{\tau}{\tau_0} e^{-\frac{t}{\tau}}. \tag{22}$$

In order to measure a 2D concentration distribution, an area of interest needs to be excited by a thin laser sheet. After the laser is turned off, the resulting phosphorescence emissions are recorded by a perpendicularly positioned intensified CCD camera, cf. Figure 3. Since only the liquid phase emits phosphorescence, the gas phase appears black in the intensity image. This fact is used for the detection of the gas-liquid interface and allows for the determination of the local film thickness. The integration of the phosphorescence emissions on the CCD chip starts at time t_0 and ends after the gating time Δt. Figure 4 illustrates the fact that the intensity of the recorded phosphorescence signal P equals the area under the decay curve. Therefore, P is given by integrating (22) from t_0 to $t_0 + \Delta t$:

$$P = \int_{t_0}^{t_0+\Delta t} I_0^* \frac{\tau}{\tau_0} e^{-t/\tau} \, dt = I_0^* \frac{\tau^2}{\tau_0} e^{-t_0/\tau} \left[1 - e^{-\Delta t/\tau}\right]. \tag{23}$$

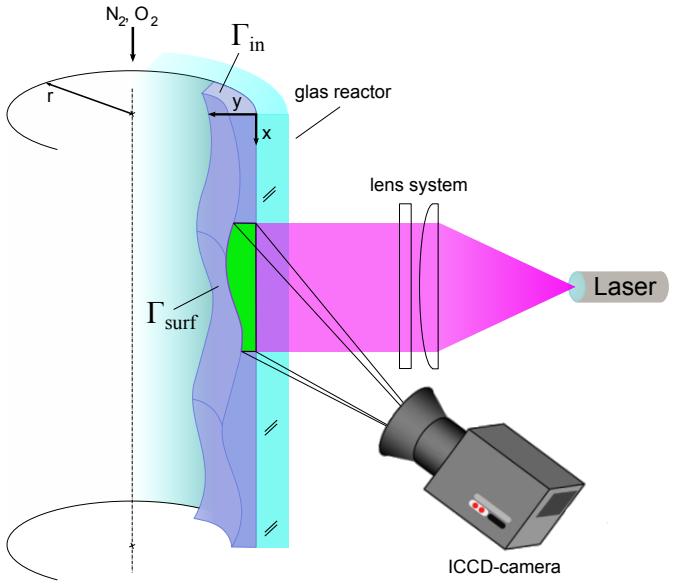

Figure 3: Scheme of Measurement technique.

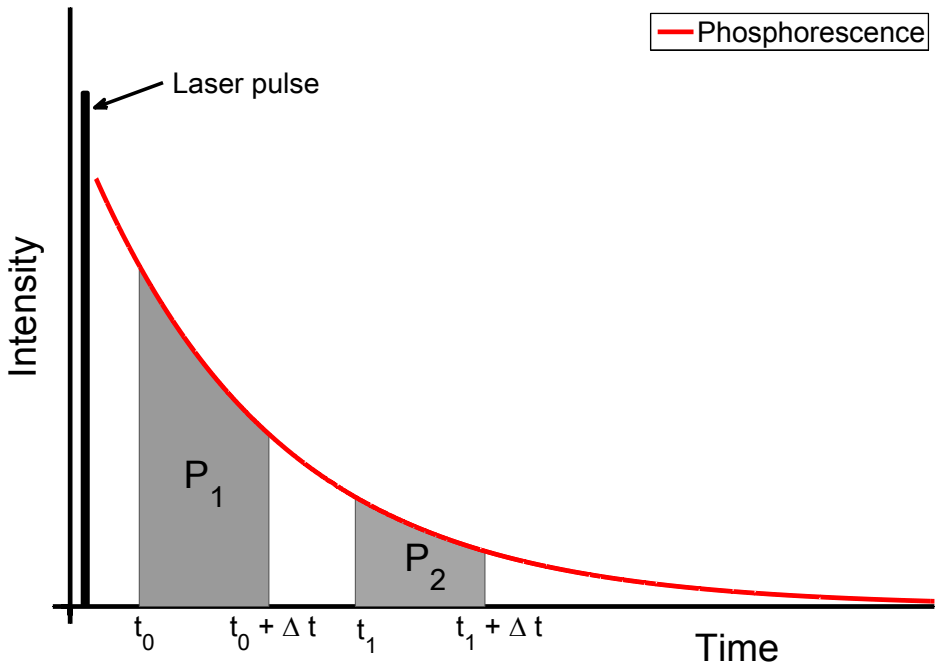

Figure 4: Scheme of double image of Pho-Signal

For quantitative measurements, the recorded images need to be corrected by a calibration image. The local incident laser energy and the influence of the optical pathway on the resulting intensity images need to be accounted for. These drawbacks can be avoided by taking two successive images (P_1 and P_2) within one phosphorescence decay curve, cf. Figure 4. This so-called ratiometric method was introduced in [12].

If the integrating time Δt is the same for both pictures, the intensity ratio of P_1 and P_2

$$\frac{P_1}{P_2} = e^{\frac{t_1 - t_0}{\tau}} \tag{24}$$

depends only on the camera settings t_0 und t_1, which mark the beginning of the integration time for picture one and picture two respectively.

Therefore, the phosphorescence lifetime can be directly calculated using

$$\tau = \frac{t_1 - t_0}{\ln\left(P_1/P_2\right)}. \tag{25}$$

By applying (25) pixel-wise on the captured double image and converting the measured lifetimes into concentrations, a 2D concentration distribution within the film can be determined using (21).

4.2 Experimental Setup

A scheme of the experimental setup of the falling film absorber is shown in Figure 5. A main reservoir contains demineralized water which was degassed with purified nitrogen 5.0. The concentration of diacetyl in the water is set to 11.4 mol/m^3.

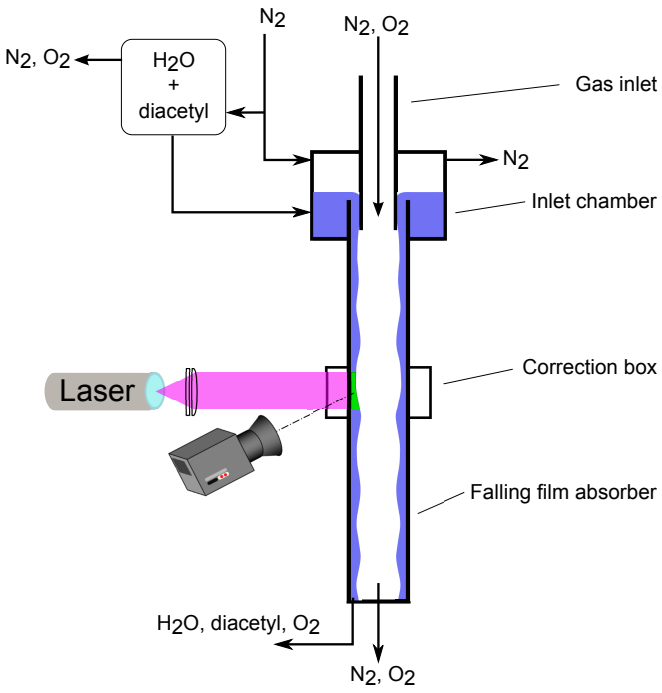

Figure 5: Scheme of the experimental setup.

The prepared liquid flows out of the main reservoir into the inlet chamber of the falling film absorber. The falling film absorber is a glass tube 1 m in length with an inner diameter of 50 mm and a wall thickness of 5 mm. The gas stream is added separately to the system through a stainless steel pipe with an outer diameter of 49 mm. By means of the inlet chamber the two tubes are mechanically connected in such a way that the gas tube is inserted concentrically into the falling film absorber. The overlapping distance of the two tubes is approximately 50 mm. This setup creates a gap of 0.5 mm between the glass and the stainless steel tube. The falling film is generated by an overflow technique (cf. Figure 5). The liquid rises in the inlet chamber just high enough to overcome the pressure loss in the small gap that creates the film. An annular film flow is created on the inside wall of the glass absorber, while the gas phase flows co-currently in the core of the glass tube.

In order to minimize optical effects due to the different refracting indices and the curvature of the glass tube, an axially movable optical correction box is applied [2]. The laser sheet optics and the camera system are positioned perpendicular to each other on a vertically adjustable platform. The ICCD system (LaVision) consists of an image intensifier (IRO, Phosphor P46, 25mm diameter, 2:1) and a CCD camera (Imager Intense, 1376 x 1040 Pixel, 20 Hz, PIV enabled). The camera lens (Micro-NIKKOR f105 mm 1:2.8) is mounted on an extension tube, with a length of 102.5 mm. The lens is equipped with a longpass filter (Schott GG 495) in order to block the exciting laser light. This setup yields an observable area of 12.7 x 8.8 mm with a spatial resolution of 8 μm per pixel. The controlling and setting of the ICCD system parameters, as well as the image acquisition is done with the DAVIS software package (LaVision). Further image processing is performed in MATLAB.

Parameter	Symbol	Value	Unit
kinematic viscosity	ν	1.0	mm^2/s
molecular diffusion coefficient	D_{mol}	0.002	mm^2/s
initial concentration	c_0	10	$kmol/mm^3$
liquid volume flow	$\dot{V}$	8	l/h

Table 1: Fluid properties used in the simulation

A nitrogen pumped laser is used as an excitation light source (LTB Berlin). At a pulse width of 700 ps each pulse has an energy of 116 μJ. The maximum repetition rate is 50 Hz. By using a 4,4 - diphenylstilbene dye (Radiant Laser Dyes) in a laser cuevette, the original nitrogen laser wavelength is shifted from 337 nm to 405 nm, at which diacetyl has an absorption maximum.

Currently, flow regimes in the range of Re = 5 - 50 can be investigated. The waviness of the falling film is induced by external vibrations. The mixing and setting of the volume flux of the gas phase is performed using two mass flow controller (ANALYT-MTC) and allows for an accurate adjustment of the gas phase composition.

5 Results

In this section, results on the model identification (with simulated data) and the experimental method are presented.

5.1 Model identification

We present first results for the source inverse problem (12). To illustrate the suitability of the proposed numerical method, it is applied to a simulated data set.

For the computational domain Ω_f defined by the film surface δ, the Nusselt flat film solution was used. For the fluid properties, we assumed water with the properties defined in Table 1.

The length l_x of the computational domain in flow direction is set to $100mm$. Since the flow properties of the film are constant in z-direction, the choice of the width $l_z = 1mm$ is arbitrary. The film height δ is set to the Nusselt height of the film, given by

$$\delta = \left(\frac{3\,\dot{V}_l\,\nu}{g} \right)^{1/3}. \tag{26}$$

The velocity field is zero in all but the x-direction. For the x-direction, it takes on the parabolic form

$$u(y) = u_N \left(2\frac{y}{l_y} - \left(\frac{y}{l_y} \right)^2 \right) \tag{27}$$

with the Nusselt velocity u_N defined as

$$u_N = \frac{g\,\delta^2}{2\,\nu}. \tag{28}$$

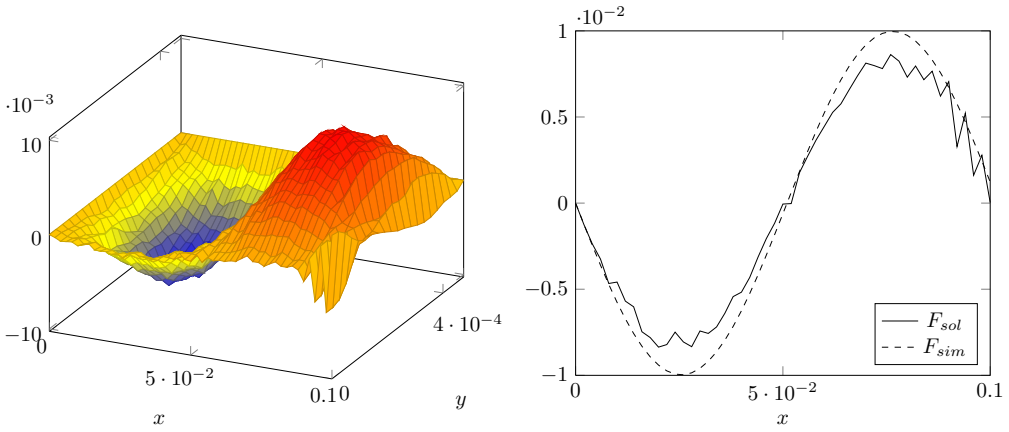

Figure 6: Quality of approximation for the first identification step of the incremental method. Left: Illustration of the resulting source distribution in the $x-y$ plane for time step $t = 0.5s$. Right: Comparison of the simulated source term F_{sim} and the solution F_{sol} after 15 CG iterations. The plot shows the values along a cut along the x axis for $y = \delta/2$, $t = 0.5s$.

The time step of the θ-method was set to $\Delta t = 0.1s$, with $\theta = 1.0$ (corresponding to implicit Euler).

A simulated source term of the form

$$F_{w,sim}(x, y, z, t) = 10^{-3} \sin(2\,\pi\ (x - t)) \sin(2\,\pi\, y)\, \frac{\text{mol}}{m^3 s}$$

was generated. Using the PDE (9), the corresponding concentration profile c_{sim} was computed. To simulate noise in measurements, perturbed measurements $\hat{c}_{sim}$ were obtained by adding Gaussian noise with zero mean and standard deviation of 10^{-3} to c_{sim}.

The source inverse problem (12) was solved using the CGNE algorithm. The stopping criterion for regularization was set to 15 iterations, which turned out to be sufficient here. All PDEs in this setup were solved using 50x20x3 grid points in x, y and z direction, and ten time steps, using the FEM solver DROPS. SUPG stabilization was used for all problems, which considerably sped up the solution of the subproblems.

In Figure 6, two plots illustrate the quality of the solution of the inverse problem. The left plot shows the solution F_{sol} in the $x-y$-plane at $z = 0.5mm$ and $t = 0.5s$. Note that due to the symmetry of the flow properties in z-direction, the solution is independent of z. The right plot shows a comparison of the solution F_{sol} (continuous line) with the true solution F_{sim} (dashed line) for the x-plane at $z = 0.5mm$, $t = 0.5s$, with $y = \frac{\delta}{2}$.

The solution of the inverse problem shows excellent agreement with the original simulated data for the region inside the computational domain. Significant errors only appear at the Dirichlet boundaries. This is due to the fact that the gradient is computed from the solution of the adjoint equation of the operator K_1. By definition of the boundary conditions of the adjoint problem, the gradient at the Dirichlet boundaries of the original problem is always zero. Therefore, no progress in fitting the model to the data can be achieved. This must be taken into consideration when fitting the model candidates in later stages of the incremental method.

Table 2: Parameters of the experimental setup

Parameter	Name	Value
Liquid flow Reynolds number / -	Re_l	16
Gas flow Reynolds number / -	Re_g	82
Liquid flow rate / l h^{-1}	$\dot{V}_l$	8
Gas flow rate / l h^{-1}	$\dot{V}_g$	180
Environmental temperature / °C	ϑ	25.7
Phosphorescence lifetime / μs	τ_0	214
Intensifier gain / %	Gain	90
Intensifier gating time / μs	Δt	200
Time between laser pulse and and start of image acquisition / μs	t_0	8
Time delay between start of each image acquisition / μs	t_1 - t_0	230

5.2 Experimental results

The experimental settings are summarized in Table 2. The images were taken 150 mm after the inlet. Prior to the actual experiments, reference images were taken to correct the distortions caused by the curvature of the glass tube. For the recording of these correction images, the falling film absorber was flooded with the water-diacetyl solution. A reference plate with a regular pattern on it was submerged into it, placed at the position of interest, and photographed. In a pre-editing image processing step, the built-in calibration routine of the camera software used these reference recordings to correct the images. Simultaneously, this correction procedure provided the required scale.

The low intensity of the phosphorescence emission requires a high gain setting for the image intensifier. This reduces the obtainable signal to noise ratio and therefore the spatial resolution. At the current development stage of the experimental setup, the images do show quantitatively if oxygen is present in the gas phase. Nevertheless, it is not possible to determine concentration distributions accurately within the film. However, with the current experimental setup, film thickness measurements are feasible. In the following only oxygen-free falling films are taken into account.

In Figure 5.2, a double image is shown as an example. Both images show the same wave, recorded successively during one decay curve within 430 μs. The red lines depict the gas/liquid interface and the position of the wall. While the position of the glass wall can be easily detected automatically, the gas/liquid interface needs to be marked manually. The halo, which can be seen above the film surface, hinders an automated surface detection. This effect is caused by scattered light originating from the excited volume. Since the excited diacetyl molecules emit light in all directions, and the light rays travel from an optical denser into a an optical thinner material, they are diffracted at the film surface away from the axis of incidence. This results in a phantom image of the wave, which appears as a halo [1]. In addition to that, the physical phenomenon of total reflection accounts for a second optical effect, which can be seen in the images. Within the wave, a non-constant intensity distribution is observed, even though no oxygen is present in the film and diacetyl is homogeneously distributed in the liquid. At the gas/liquid interface the intensity distribution reaches its maximum and the film surface is identifiable. Nevertheless, if for each pixel of this double image the phosphorescence lifetime τ is calculated with (24), these effects are cancelled out. This can be explained by the fact, that the recorded light is solely the diacetyl phosphorescence, which originates from

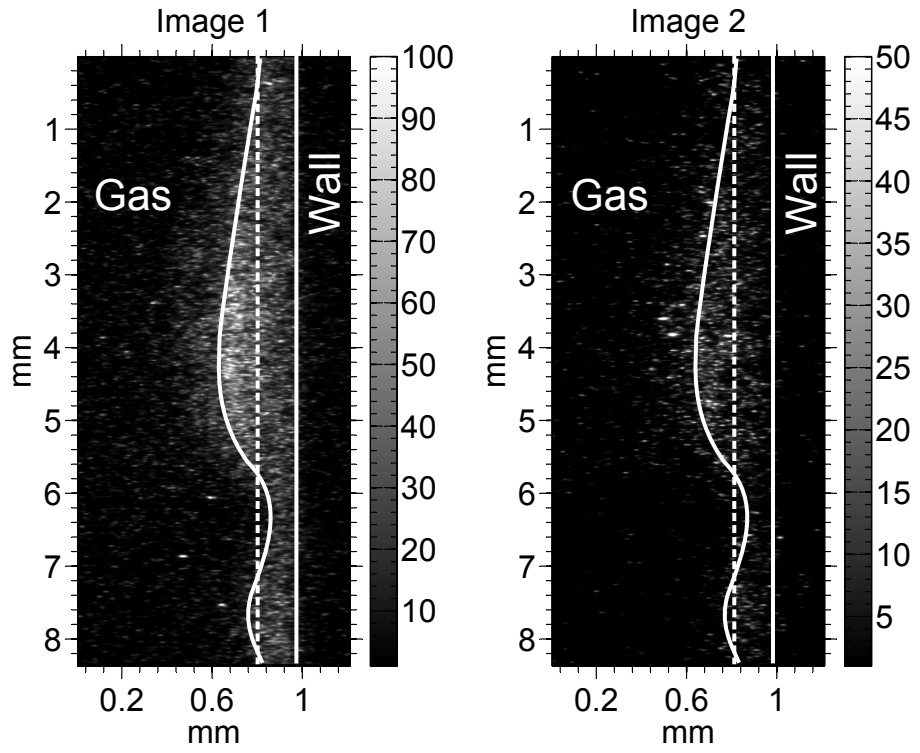

Figure 7: Two successive intensity images of an oxygen-free falling film are shown. The captured pictures were taken within one phosphorescence decay curve. The corresponding experimental setup is given in Table 2. Red lines: Position of the Wall and the film surface; green line: calculated Nusselt film thickness ($\delta_{Nu_{Mean}} = 163\,\mu$m). All lines were added manually.

within the excited volume element.

In the presented image, the measured maximum, minimum and mean film thicknesses are $\delta_{max} = ...$, $\delta_{min} = ...$ and $\delta_{mean} = ...$. The average lifetime τ within the wave was .... .

6 Conclusions

This collaborative research effort focuses on the development of a powerful but computationally manageable model for mass transfer in liquid falling films. The first step of the systematic derivation of a model structure by means of the incremental model identification method has been completed. To achieve this, suitable efficient techniques have been implemented in the software package DROPS. The introduced experimental method was used to measure film thickness.

Current work in our group focuses on the further development of the modeling, numerical simulation and experimental methods. The modeling efforts continue along the path of the incremental method. For the solution of the PDEs on wavy computational domains, defined by long wave evolution equations, the ALE method will be implemented in DROPS. Further improvements are incorporated into the experimental measuring method to overcome the

limitations due to the low phosphorescence intensity.

Symbol	Description
D_{eff}	Effective diffusion coefficient
D_{mol}	Molecular diffusion coefficient
D_{w}	Diffusion due to waves
F_{w}	Wavy source term
c	concentration
c_m	Measured concentration
$\mathbf{u}$	velocity profile
$\mathbf{J}$	generalized molecular flux
$\mathbf{J}_D$	molecular flux due to diffusion
f_w	model for D_{w}
θ	parameters
K_1, K_2	Operators
$\mathcal{L}^2$	Lebesgue space of square-integrable functions
Ω_f	Time-dependent computational domain
$\hat{\Omega}$	Fixed reference computational domain
δ	film height
x	coordinate in direction of film flow
y	coordinate in direction of film height
z	coordinate in direction of film width
t	time
$\dot{V}_l$	liquid volume flow

References

[1] Adomeit, P. *Experimentelle Untersuchung der Strömung laminar-welliger Rieselfilme.* PhD thesis, RWTH Aachen, 1996.

[2] Adomeit, P., and Renz, U. Hydrodynamics of three-dimensional waves in laminar falling films. *Int. J. Multiphase Flow 26* (2000), 1183–1208.

[3] Bänsch, E. Stabilized space-time finite element formulations for free-surface flows. *Numer. Math. 88* (2001), 203–235.

[4] Brauer, H. Stoffaustausch beim Rieselfilm. *Chemie-Ing. - Techn 30*, 2 (1958), 75–84.

[5] Brooks, A., and Hughes, T. Streamline upwind/Petrov-Galerkin formulations for convection dominated flows with particular emphasis on the incompressible Navier-Stokes equations. *Comput. Methods Appl. Mech. Engrg. 32* (1982).

[6] Donea, J., and Huerta, A. *Finite Element Methods for Flow Problems.* John Wiley & Sons, 2003.

[7] DROPS package. `http://www.igpm.rwth-aachen.de/DROPS/`.

[8] Engl, H. W., Hanke, M., and Neubauer, A. *Regularization of Inverse Problems.* Kluwer Academic Publishers, Dordrecht, 1996.

[9] Frenkel, A. L., and Indireshkumar, K. Wavy film flows down an inclined plane: Perturbation theory and general evolution equation for the film thickness. *Phys. Rev. E 60*, 4 (Oct 1999), 4143–4157.

[10] Gross, S., and Reusken, A. *Numerical Methods for Two-phase Incompressible Flows*, vol. 40 of *Springer Series in Computational Mathematics*. Springer, 2011.

[11] Hanke, M. *Conjugate Gradient Type Methods for Ill-Posed Problems*. Longman Scientific & Technical, 1995.

[12] Hu, H., and Koochesfahani, M. A novel technique for quantitative temperature mapping in liquid by measuring the lifetime of laser induced phosphorescence. *Journal of Visualization 6*, 2 (Jan. 2003), 143–153.

[13] Karalashvili, M. *Incremental Identification of Transport Phenomena In Laminar Wavy Film Flows*. PhD thesis, RWTH Aachen University, 2011. to appear.

[14] Karalashvili, M., Gross, S., Mhamdi, A., Marquardt, W., and Reusken, A. Identification of transport coefficient models in convection-diffusion equations. *SIAM J. Sci. Comput. 33*, 1 (2011), 303–327.

[15] Karalashvili, M., Gross, S., Mhamdi, A., Reusken, A., and Marquardt, W. Incremental identification of transport coefficients in convection-diffusion systems. *SIAM J. Sci. Comput. 30*, 6 (2008), 3249–3269.

[16] Karalashvili, M., Mhamdi, A., Dietze, G. F., Bücker, H. M., Vehreschild, A., Kneer, R., Bischof, C. H., and Marquardt, W. Sensitivity analysis and identification of an effective heat transport model in wavy liquid films. In *Progress in Computational Heat and Mass Transfers, Guangzhou, China* (2009), pp. 644–651.

[17] Löffler, K., Gambaryan-Roisman, T., and Stephan, P. Wave patterns in thin films flowing down inclined smooth and structured planes. In *Proceedings of th 6th International Conference on Multiphase Flow* (July 2007).

[18] M., B. Stabilized space-time finite element formulations for free-surface flows. *Communications in Numerical Methods in Engineering 11* (2001), 813–819.

[19] Marquardt, W. *Towards a process modeling methodology*, vol. 293 of *R. Berber: Methods of Model-Based Control, NATO-ASI Ser. E, Applied Sciences, Kluwer Academic Pub., Dordrecht*. Kluwer Academic Pub, 1995, pp. 3–41.

[20] Marquardt, W. Model-based experimental analysis of kinetic phenomena in multiphase reactive systems. *Chem. Eng. Res. Des. 83*, A6 (2005), 561–573.

[21] Mudunuri, R. R., and Balakotaiah, V. Solitary waves on thin falling films in the very low forcing frequency limit. *AIChE Journal 52*, 12 (2006), 3995–4003.

[22] Panga, M. K. R., Mudunuri, R. R., and Balakotaiah, V. Long-wavelength equation for vertically falling films. *Phys Rev E Stat Nonlin Soft Matter Phys 71* (2005), 36310–36311.

[23] Ruyer-Quil, C., and Manneville, P. Improved modeling of flows down inclined planes. *Eur. Phys. J. B 15* (2000), 357–369.

[24] Saad, Y., and Schultz, M. H. GMRES: A generalized minimal residual algorithm for solving nonsymmetric linear systems. *SIAM J. Sci. Statist. Comput. 7* (1986), 856–869.

[25] Schagen, A., and Modigell, M. Luminescence technique for the measurement of local concentration distribution in thin liquid films. *Experiments in Fluids 38*, 2 (Feb. 2005), 174–184.

[26] Schagen, A., and Modigell, M. Local film thickness and temperature distribution measurement in wavy liquid films with a laser-induced luminescence technique. *Experiments in Fluids 43*, 2 (Aug. 2007), 209–221.

[27] Trevelyan, P., and Kalliadasis, S. Wave dynamics on a thin-liquid film falling down a heated wall. *Journal of Engineering Mathematics 50* (2004), 177–208. 10.1007/s10665-004-1016-x.